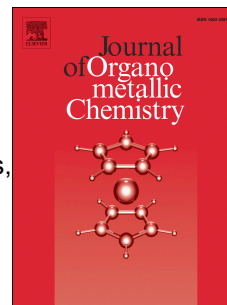


Accepted Manuscript

Pyridyl- and Pyrimidyl-Phosphine-Substituted [FeFe]-Hydrogenase Mimics: Synthesis, Characterization and Properties

Hong-Hua Cui, Nan-Nan Wu, Jin-Yun Wang, Ming-Qiang Hu, Hui-Min Wen, Chang-Neng Chen



PII: S0022-328X(14)00208-3

DOI: [10.1016/j.jorganchem.2014.04.026](https://doi.org/10.1016/j.jorganchem.2014.04.026)

Reference: JOM 18561

To appear in: *Journal of Organometallic Chemistry*

Received Date: 5 March 2014

Revised Date: 22 April 2014

Accepted Date: 27 April 2014

Please cite this article as: H.-H. Cui, N.-N. Wu, J.-Y. Wang, M.-Q. Hu, H.-M. Wen, C.-N. Chen, Pyridyl- and Pyrimidyl-Phosphine-Substituted [FeFe]-Hydrogenase Mimics: Synthesis, Characterization and Properties, *Journal of Organometallic Chemistry* (2014), doi: 10.1016/j.jorganchem.2014.04.026.

This is a PDF file of an unedited manuscript that has been accepted for publication. As a service to our customers we are providing this early version of the manuscript. The manuscript will undergo copyediting, typesetting, and review of the resulting proof before it is published in its final form. Please note that during the production process errors may be discovered which could affect the content, and all legal disclaimers that apply to the journal pertain.

Pyridyl- and Pyrimidyl-Phosphine-Substituted [FeFe]- Hydrogenase Mimics: Synthesis, Characterization and Properties

Hong-Hua Cui,^{‡a,b} Nan-Nan Wu,^{‡a,b} Jin-Yun Wang,^a Ming-Qiang Hu,^a Hui-Min Wen,^a and
Chang-Neng Chen^{*a}

^a State Key Laboratory of Structural Chemistry, Fujian Institute of Research on the Structure of Matter, Chinese Academy of Sciences, Fuzhou 350002, P. R. China. ^b University of Chinese Academy of Sciences, Beijing, 100039, P. R. China

Highlight: 1) Pyrimidyl-diphosphine substituted [Fe₂S₂] mimics have been firstly synthesized. 2) The pyrimidyl-diphosphine ligand PNNP can affect the features of LUMOs when both of the P atoms are coordinated to [Fe₂S₂] units.

Abstract: Two tetranuclear iron-sulfur complexes {[(μ -pdt)Fe₂(CO)₅]₂(PNP) (**2**) and [(μ -pdt)Fe₂(CO)₅]₂(PNNP) (**3**)} and three dinuclear ones {[(μ -pdt)Fe₂(CO)₅](PNP) (**4**), [(μ -pdt)Fe₂(CO)₅](PNNP) (**5**) and [(μ -pdt)Fe₂(CO)₅](PNN) (**6**)} were synthesized, using two new pyrimidyl-phosphine ligands PNNP [4,6-bis(diphenylphosphino) pyrimidine] and PNN (4-

*Corresponding author. Tel: +86 591 83792395; fax: +86 591 83792395

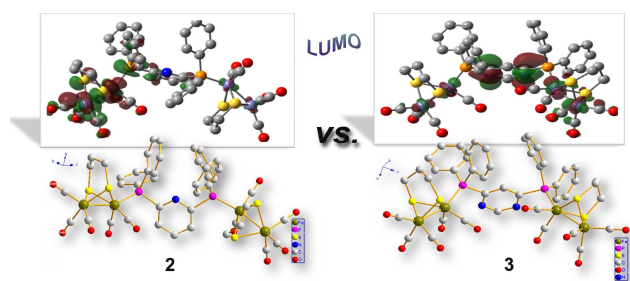
E-mail address: ccn@fjirsm.ac.cn

[‡]H.-H. Cui and N.-N. Wu contributed equally.

tertiary butyl-6-diphenylphosphino pyrimidine) together with the reported pyridyl-phosphine PNP [bis(diphenylphosphino)pyridine] as substituents to react with $\text{Fe}_2(\mu\text{-pdt})(\text{CO})_6$. The molecular structures of **2**, **3** and **6** were confirmed by single-crystal X-ray analyses, which show that all phosphine ligands occupy the apical positions, while the space group of **3** ($P21/n$) is different from that of **2** ($P-1$). Cyclic voltammograms reveal that pyrimidyl-phosphine substituted complexes **3**, **5** and **6** present two reduction waves in CH_2Cl_2 solutions, while pyridyl-phosphine substituted **2** and **4** show only one. The DFT computational studies demonstrate that the contributions to the LUMO of **3** are comparable from the two Fe_2S_2 centers and ligated PNNP ligand, which is different from those of other $[\text{Fe}_2\text{S}_2]$ mimics in this work.

Graphical abstract

The contributions to the LUMO of **3** are comparable from the two $[\text{Fe}_2\text{S}_2]$ centers and the ligated PNNP, which is different from other $[\text{Fe}_2\text{S}_2]$ mimics, such as complex **2**.



Keywords: Pyrimidyl-diphosphine ligand; $[\text{FeFe}]$ hydrogenase; Tetranuclear iron-sulfur complexes.

1. Introduction

Over the past decade, intense work has been done aiming at developing effective bioinspired complexes of the active site of $[\text{FeFe}]$ -hydrogenase for H_2 generation.[1-2] In the known

synthetic models, electron-donating phosphine ligands have been widely used by the replacement of carbonyl ligands to mimic the CN- ligation on the Fe sites in order to prepare more stable diiron models and avoid polymerization of the diiron units.[3-7] Among the phosphine ligands, bisphosphine are capable of giving several coordination modes of substituted diiron complexes, such as bridging-form symmetric and chelating-form asymmetric isomers as well as pendant-form and bridging-form intermolecular modes, which depend on the nature of the bidentate phosphines and reaction conditions.[8-9] Many studies have been carried out on the asymmetry of the diiron centre, or mixed valence Fe(I)-Fe(II) assemblies about the bisphosphine-substituted Fe₂S₂ derivatives.[10-11] The bisphosphine used in these studies are mainly the flexible ones, such as dpmm (bis(diphenylphosphino)methane) and dppe (1,2-bis(diphenylphosphino)ethane). By comparison, rigid bidentate phosphine ligands are less employed.[12-13] In addition, the introduction of a rigid and conjugate disulfide bridge to the diiron complexes makes the electrochemical properties different from that with flexible bridges.[14-17] Keeping these in mind, we aim to explore [Fe₂S₂] complexes using rigid bisphosphine ligands as bridges.

Bis(diphenylphosphino)pyridine (PNP) is widely used in preparing homonuclear or heteronuclear metal complexes due to the presence of two different coordination sites, N and P atoms.[18-19] It is appealing to us that the basic nitrogen atom may act as a proton relay and the diphosphine-pyridine may result in different properties from other pyridyl-phosphine ligands, which contain only one P atom.[20-21] Here we select PNP as a bridge to link Fe₂S₂ centers to study the influence of aromatic ring on the multinuclear iron-sulfur complexes. Moreover, complexes containing pyrimidyl-phosphine are rare compared with pyridyl-phosphine ligands. For the stronger electron-withdrawing inductive and conjugative effects of the N atoms in pyrimidine than that in pyridine,[22] pyrimidyl-phosphine may exhibit different properties in

iron-sulfur complexes. Thus, we designed and synthesized two new pyrimidyl-phosphine ligands, PNNP (4, 6-bis(diphenylphosphino) pyrimidine) and PNN (4-tertiary butyl -6-diphenylphosphino pyrimidine). Using the three above ligands as substituents, two tetranuclear iron-sulfur complexes $[(\mu\text{-pdt})\text{Fe}_2(\text{CO})_5]_2(\text{PNP})$ (**2**) and $[(\mu\text{-pdt})\text{Fe}_2(\text{CO})_5]_2(\text{PNNP})$ (**3**) and three dinuclear ones $[(\mu\text{-pdt})\text{Fe}_2(\text{CO})_5](\text{PNP})$ (**4**), $[(\mu\text{-pdt})\text{Fe}_2(\text{CO})_5](\text{PNNP})$ (**5**) and $[(\mu\text{-pdt})\text{Fe}_2(\text{CO})_5](\text{PNN})$ (**6**) were obtained. The preparations and characterizations of complexes **2-6**, and the molecular structures of **2**, **3** and **6** are presented. We mainly focus on the discussion of the properties of **2**, **3** and **6** in this work. Importantly, the DFT computational studies of **2-6** show the differences between complex **3** and other four complexes on the components of molecular orbitals (MOs).

2 Experimental

2.1 Materials

All reactions and operations were performed under dry oxygen-free nitrogen atmosphere with standard Schlenk techniques. Solvents used were dried and distilled according to the standard methods. $\text{Fe}_2(\mu\text{-pdt})(\text{CO})_6$, [23] and 2,6-bis(diphenylphosphino)pyridine (PNP) [19] were prepared according to literature procedures and other materials were obtained commercially and used without further purification. Infrared spectra were obtained on a Perkin–Elmer Spectrum One FTIR spectrometer with KBr pellets. NMR spectra were carried out on a Bruker Avance III (400 MHz) spectrometer. Elemental analyses were recorded on a Perkin–Elmer model 240 C elemental analyzer. Electrospray ionization mass spectrometry was performed on a Finnigan LCQ mass spectrometer.

2.2 Electrochemistry

The cyclic voltammograms (CV) were carried out using a CH instruments Model 630A Electrochemical Workstation in CH₂Cl₂ or CH₂Cl₂/DMF mixed solutions containing 0.1 M (Bu₄N)PF₆ as the supporting electrolyte. All electrochemical measurements were performed at a scan rate of 100 mV·s⁻¹ in the cathodic direction in a three-electrode cell under Ar atmosphere. The potential was measured against a reference electrode Ag/AgCl, a 3 mm diameter glassy carbon working electrode and a platinum counter electrode with the ferrocenium/ferrocene (Fc⁺/Fc) as an internal reference and all potentials in the present work are referred to the Fc⁺/Fc potential.

2.3. X-ray crystallography

Single-crystal X-ray diffraction data of complexes **2** and **6** were measured on a Saturn70 diffractometer equipped with a graphite-monochromated Mo K_α radiation ($\lambda = 0.71073 \text{ \AA}$) at the temperature of 293 K and the data of **3** was collected on a SuperNova, Dual, Mo K_α radiation, Atlas diffractometer at 293 K. Data collection, refinement and reduction were performed by CRYSTALCLEAR program.[24] The structures were solved by direct methods with SHELXS-97[25] and refined by full-matrix least-squares methods using the SHELXTL-97 program package on F^2 . Detailed crystallographic data and structural refinements information are summarized in Table 1.

Table 1 Crystal data and structure refinement details for complexes **2**, **3** and **6**.

Complexes	2	3 ·2H ₂ O	6 ·H ₂ O
Molecule formula	Fe ₄ S ₄ C ₄₅ H ₃₅ NO ₁₀ P ₂	Fe ₄ S ₄ C ₄₄ H ₃₈ N ₂ O ₁₂ P ₂	Fe ₂ S ₂ C ₂₈ H ₂₉ N ₂ O ₆ P
Formula weight	1163.32	1200.35	696.32
T (K)	293(2)	293(2)	293(2)
Crystal system	Triclinic	monoclinic	Triclinic

Space group	<i>P</i> -1	<i>P</i> 21/ <i>n</i>	<i>P</i> -1
a (Å)	9.141(2)	11.3590(5)	9.210(10)
b (Å)	10.283(2)	25.8540(12)	10.936(12)
c (Å)	27.772(7)	18.9642(8)	18.68(2)
α (°)	95.684(9)	90	74.39(5)
β (°)	92.450(7)	92.046(4)	77.10(5)
γ (°)	108.656(7)	90	73.15(5)
V (Å ³)	2439.6(9)	5565.8(4)	1713(3)
Z	2	4	2
Dcalc (g·cm ⁻³)	1.584	1.428	1.340
R1 ^a / wR2 ^b (I > 2 σ (I))	0.0531/0.1423	0.0441/0.1387	0.0719/0.2121
R1 ^a / wR2 ^b (all data)	0.0850/0.1780	0.0529/0.1484	0.1027/0.2400
GOF on F ²	1.063	1.092	0.942

$${}^a R1 = \frac{\sum ||F_o| - |F_c||}{\sum |F_o|}, \quad {}^b wR2(F_o^2) = \frac{[\sum w(F_o^2 - F_c^2)^2 / \sum w(F_o^2)^2]}{1/2}.$$

2.4. Theoretical calculations

In order to get an insight into the electronic properties of the investigated complexes **2-6**, the calculations were implemented by using Gaussian 03 program package.[26] The density functional theory (DFT) with the hybrid Becke three-parameter Lee-Yang-Parr (B3LYP) functional[27-28] was firstly employed for the optimization of the geometrical structures in vacuum. The initial structures of **2**, **3** and **6** were extracted from the crystallographically determined geometries, and **4**, and **5** were cut out from **2** and **3**, respectively. The optimized structures of complexes **2-6** and the protonated [**2-H_N**], [**3-2H_N**] and [**6-2H_N**] are shown in Figure S1 in the Supporting Information. During the optimization processes, the convergent values of maximum force, root-mean-square (RMS) force, maximum displacement, and RMS displacement were set by default. To precisely describe the electronic properties, the single-point

DFT calculations were performed based on the optimized structures by considering the solvent effects of dichloromethane solutions in the help of conductor-like polarizable continuum model method (CPCM).[29-30] All of the calculations were implemented at the 6-31G* basis set level. Visualization of the optimized structures and frontier molecular orbitals were performed by GaussView. Ros & Schuit method (C-squared population analysis method, SCPA)[31] is supported to partition orbital composition analysis by using Multiwfn 2.4 program.[32]

2.5 Synthesis

2.5.1. Synthesis of 4, 6-bis(diphenylphosphino)pyrimidine (PNNP)

Compound diphenylphosphine (Ph_2PH) (2.0mL, 11mmol) in dry tetrahydrofuran (THF) (20 mL) was added to the THF solution containing excess lithium (0.152 g, 20mmol) in ice bath. Then the mixture was warmed to the room temperature and refluxed for 2 hours. After cooling down, the red solution was added dropwise to the solution of 4,6-dichloropyrimidine (0.9 g, 5 mmol) in THF (10 mL) at 0 °C. The new pale yellow mixture was then stirred at 40 °C until the reaction was completely finished. Saturated NH_4Cl solution was added after the solvent was evaporated. The aqueous phase was extracted with dichloromethane (3*50 mL) and the organic phase was dried with anhydrous Na_2SO_4 overnight. After solvent was removed, the crude product was purified by chromatography on silica gel (100-200) with dichloromethane/petroleum (3:1 v/v) and dichloromethane as gradient eluent to give an off-white solid. The yield was 1.42 g (63.1%). Anal. Calcd. for $\text{C}_{28}\text{H}_{22}\text{N}_2\text{P}_2$: C, 74.99%; H, 4.94%; N, 6.25%. Found: C, 75.06%; H, 4.82%; N, 6.17%. ESI-MS calculated for $\text{C}_{28}\text{H}_{22}\text{N}_2\text{P}_2$, found $[\text{M}+\text{H}]^+$: 449.6. ^1H NMR (400 MHz, DMSO): δ 9.16 (s, 1H), 7.42 – 7.27 (m, 20H), 6.60 (s, 1H). ^{31}P NMR (162MHz, DMSO): δ -4.45 (s).

2.5.2. Synthesis of 4-tertiary butyl-6-diphenylphosphino pyrimidine (PNN)

A solution of tert-BuLi in hexane (2.5M, 6.0 mL) was dropwised slowly to the solution of Ph₂PH (10 mmol, 1.8 mL) in tetrahydrofuran (30 mL) at -78 °C. The resulting mixture was stirred for one hour and warmed slowly to 0 °C. Then the red solution was transferred dropwise to the THF solution of 4,6-dichloropyrimidine (1.5 g, 10 mmol). After stirring for one hour at this temperature, the mixture was warmed to the room temperature for another 5 hours. The solvent was removed in vacuum and saturated NH₄Cl solution was added. The aqueous phase was extracted with dichloromethane (3*40 mL) and the organic phase was dried with anhydrous Na₂SO₄ overnight. After solvent was removed, the crude product was purified by chromatography on silica gel (100-200) with dichloromethane/petroleum (3:2 v/v) and dichloromethane as gradient eluent to give off-white products PNN and PNNP. The yields of them were 1.10 g (34.4%) and 1.17 g (52%), respectively. Anal. Calcd for C₂₀H₂₁N₂P: C, 74.98%; H, 6.61%; N, 8.74%. Found: C, 74.85%; H, 6.70%; N, 8.68%. ESI-MS calculated for C₂₀H₂₁N₂P, found [M+H]⁺: 321.2. ¹H NMR (400 MHz, DMSO): δ 8.89 (s, 1H), 7.37 – 7.24 (m, 10H), 7.19 (s, 1H), 3.42 (s, 9H). ³¹P NMR (162 MHz, DMSO) δ -3.06 (s).

2.5.3. Synthesis of [(μ-pdt)Fe₂(CO)₅]₂(PNP) (**2**)

A solution of Fe₂(μ-pdt)(CO)₆ (0.780 g, 2 mmol) and Me₃NO·2H₂O (0.244 g, 2.2 mmol) in 20 ml acetonitrile was stirred for 15 min at room temperature. Then the ligand bis(diphenylphosphino)pyridine (0.449 g, 1mmol) was added and the reaction mixture was stirred for 12 hours at room temperature. The resulted solution was evaporated under reduced pressure. The residue was purified by chromatography on silica gel (100-200) with dichloromethane/petroleum (3:2 v/v) as eluent to give a red solid. The yield was 0.806 g (69.3%). The crystals of **2** suitable for X-ray crystallography study were grown upon slow diffusion of hexane into a dichloromethane solution containing **2** at 4 °C. Anal. Calcd. for

$\text{Fe}_4\text{S}_4\text{C}_{45}\text{H}_{35}\text{NO}_{10}\text{P}_2$: C, 46.46%; H, 3.03%; N, 1.20%. Found: C, 46.53%; H, 3.27%; N, 1.14%. ESI-MS calculated for $\text{Fe}_4\text{S}_4\text{C}_{45}\text{H}_{35}\text{NO}_{10}\text{P}_2$, found [M]: 1163.8. IR (KBr, cm^{-1}): $\nu(\text{CO})$ 2043, 1978, 1932. ^1H NMR (400 MHz, DMSO): δ 8.12 (s, 1H), 7.81 (s, 2H), 7.63 – 7.29 (m, 20H), 1.77 – 1.64 (m, 4H), 1.26 (s, 6H), 1.05 (s, 2H). ^{31}P NMR (162MHz, DMSO): δ 66.84 (s).

2.5.4. Synthesis of $[(\mu\text{-pdt})\text{Fe}_2(\text{CO})_5]_2(\text{PNNP})$ (**3**)

The product was synthesized in the similar way as **2**, except that the ligand PNNP (0.449 g, 1mmol) was added instead of PNP. The crude product was purified by column chromatography on silica gel (100-200) with dichloromethane/petroleum (1:1 v/v) as eluent to give **3** as a red solid. The yield was 0.838 g (72%). Diffusion of hexane into the dichloromethane solution containing **3** at 4 °C gave the crystals suitable for X-ray crystallography study. Anal. Calcd. for $\text{Fe}_4\text{S}_4\text{C}_{44}\text{H}_{34}\text{N}_2\text{O}_{10}\text{P}_2$: C, 45.39%; H, 2.94%; N, 2.41%. Found: C, 45.73%; H, 3.12%; N, 2.64%. ESI-MS calculated for $\text{Fe}_4\text{S}_4\text{C}_{44}\text{H}_{34}\text{N}_2\text{O}_{10}\text{P}_2$, found [M]: 1164.2. IR (KBr, cm^{-1}): $\nu(\text{CO})$ 2044, 1983, 1937. ^1H NMR (400 MHz, DMSO): δ 9.66 (s, 1H), 7.68 – 7.61 (m, 8H), 7.53 (dq, $J = 14.2$, 7.1 Hz, 12H), 7.09 (s, 1H), 1.76 (d, $J = 10.3$ Hz, 4H), 1.46 (s, 6H), 1.25 (s, 2H). ^{31}P NMR (162MHz, DMSO): δ 67.48 (s).

2.5.5. $[(\mu\text{-pdt})\text{Fe}_2(\text{CO})_5](\text{PNP})$ (**4**)

The product was obtained following the same synthetic strategy as **2**, except that one equivalent $\text{Fe}_2(\mu\text{-pdt})(\text{CO})_6$ (0.388 g, 1 mmol) was used. The crude product was purified by column chromatography on silica gel (100-200) with dichloromethane/petroleum (2:1 v/v) as eluent to give **4** as the main product. The yield was 0.475 g (59%). Anal. Calcd. for $\text{Fe}_2\text{S}_2\text{C}_{37}\text{H}_{29}\text{NO}_5\text{P}_2$: C, 55.18%; H, 3.63%; N, 1.74%. Found: C, 55.09%; H, 3.78%; N, 1.67%. ESI-MS calculated for $\text{Fe}_2\text{S}_2\text{C}_{37}\text{H}_{29}\text{NO}_5\text{P}_2$, found [M]: 805.6. IR (KBr, cm^{-1}): $\nu(\text{CO})$ 2042, 1979, 1956, 1930. ^1H NMR (400 MHz, DMSO): δ 8.12 (s, 1H), 7.82 (s, 2H), 7.59 (d, $J = 8.1$ Hz, 4H), 7.48 (d, $J = 6.8$ Hz,

6H), 7.39 (s, 4H), 7.35 – 7.30 (m, 8H), 1.70 (s, 3H), 1.43 (d, $J = 13.6$ Hz, 2H), 1.24 (s, 1H). ^{31}P NMR (162 MHz, DMSO): δ 65.72 (s), -4.14 (s).

2.5.6. Synthesis of $[(\mu\text{-pdt})\text{Fe}_2(\text{CO})_5](\text{PNNP})$ (**5**)

The product was obtained following the same synthetic strategy as **3**, except that one equivalent $\text{Fe}_2(\mu\text{-pdt})(\text{CO})_6$ (0.388 g, 1 mmol) was used. Red solid was obtained and the yield was 0.492 g (61%). Anal. Calcd for $\text{Fe}_2\text{S}_2\text{C}_{36}\text{H}_{28}\text{N}_2\text{O}_5\text{P}_2$: C, 53.62%; H, 3.59%; N, 3.47%. Found: C, 53.51%; H, 3.74%; N, 3.38%. ESI-MS calculated for $\text{Fe}_2\text{S}_2\text{C}_{37}\text{H}_{28}\text{N}_2\text{O}_5\text{P}_2$, found $[\text{M}]$: 806.4. IR (KBr, cm^{-1}): $\nu(\text{CO})$ 2044, 1982, 1955, 1931. ^1H NMR (400 MHz, DMSO): δ 9.40 (s, 1H), 7.67 – 7.26 (m, 20H), 6.88 (s, 1H), 1.75 (d, $J = 10.6$ Hz, 3H), 1.46 (s, 2H), 1.24 (s, 1H). ^{31}P NMR (162 MHz, DMSO): δ 66.51 (s), -3.76 (s).

2.5.7. $[(\mu\text{-pdt})\text{Fe}_2(\text{CO})_5](\text{PNN})$ (**6**)

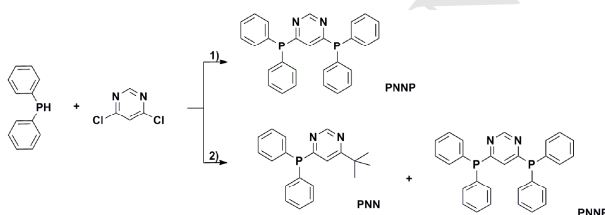
A solution of $\text{Fe}_2(\mu\text{-pdt})(\text{CO})_6$ (0.339 g, 1 mmol) and $\text{Me}_3\text{NO}\cdot 2\text{H}_2\text{O}$ (0.122 g, 1.1 mmol) in 15 ml acetonitrile was stirred for 10 minutes at room temperature. Then the ligand PNN (0.321 g, 1mmol) was added and the reaction mixture was stirred for 12 hours at room temperature. The resulted solution was evaporated under reduced pressure. The resulted residue was purified by chromatography on silica gel (100-200) with dichloromethane/petroleum (1:3 v/v) and dichloromethane gradient eluent to give **6** as a red solid. The yield was 0.471 g (69.3%). The crystals of **6** suitable for X-ray crystallography study were grown upon diffusion of diethyl ether into a dichloromethane-methanol mixed solution containing **6** at 4 °C. Anal. Calcd for $\text{Fe}_2\text{S}_2\text{C}_{28}\text{H}_{27}\text{N}_2\text{O}_5\text{P}$: C, 49.58%; H, 4.01%; N, 4.13%. Found: C, 49.52%; H, 4.10%; N, 4.17%. ESI-MS calculated for $\text{Fe}_2\text{S}_2\text{C}_{28}\text{H}_{27}\text{N}_2\text{O}_5\text{P}$, found $[\text{M}+\text{H}]^+$: 679.7. IR (KBr, cm^{-1}): $\nu(\text{CO})$ 2049, 1980, 1954, 1932. ^1H NMR (400 MHz, DMSO): δ 9.65 (s, 1H), 8.05 (d, $J = 2.6$ Hz, 1H), 7.85 –

7.78 (m, 4H), 7.63 (d, $J = 5.7$ Hz, 6H), 3.59 (s, 9H), 1.86 – 1.77 (m, 2H), 1.48 – 1.35 (m, 3H), 1.17 (s, 1H). ^{31}P NMR (162MHz, DMSO): δ 73.01 (s).

3 Results and discussions

3.1. Preparation and spectroscopic characterization of complexes

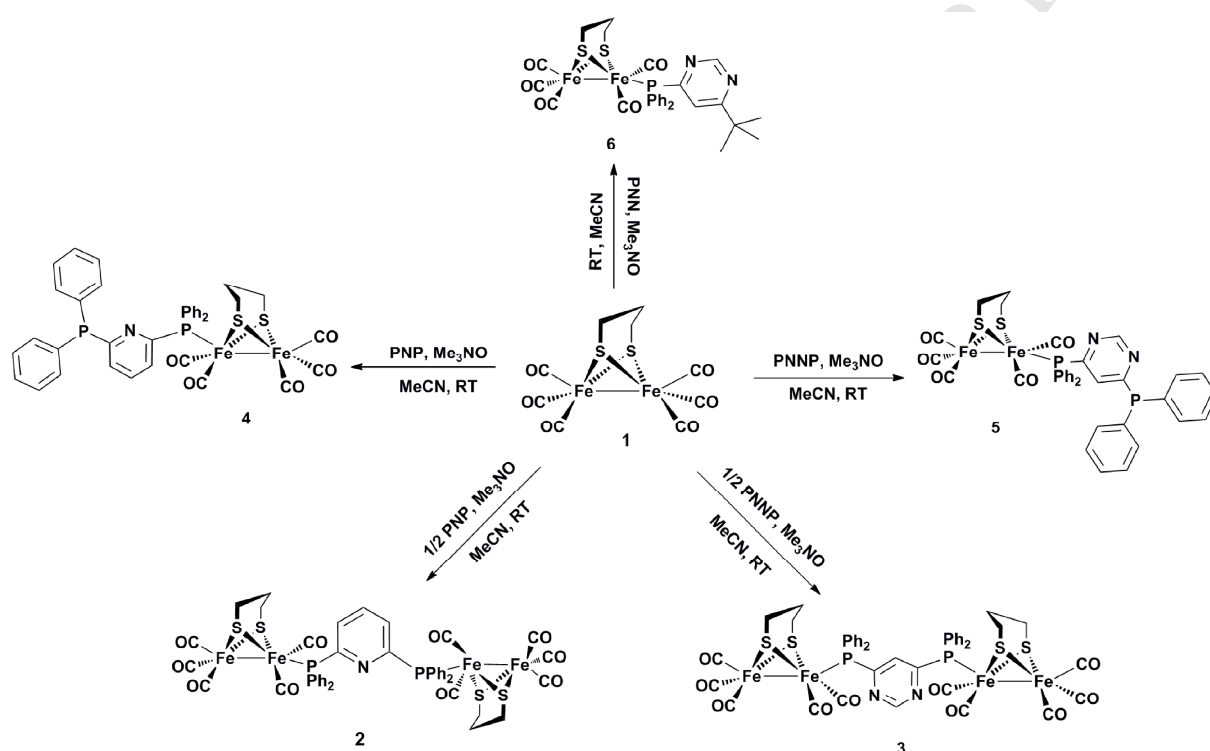
The new ligand 4,6-bis(diphenylphosphino)pyrimidine (PNNP) was obtained by the reaction of 4,6-dichloropyrimidine with two equivalent lithium diphenylphosphide (Ph_2PLi), which was prepared by diphenylphosphine (Ph_2PH) and lithium in dry, oxygen-free tetrahydrofuran as shown in Scheme 1. If one equivalent Ph_2PH was added using Li as base, the resulting product



Scheme 1 Synthetic routes for ligands PNNP and PNN. Reagents and conditions: 1) THF, Li, 0 °C; 2) THF, *tert*-BuLi, -78 °C.

was also the diphosphine ligand, PNNP, with unreacted 4,6-dichloropyrimidine. Changing the dropping order of the reactants or further lowering the ratio of Ph_2PH to 4,6-dichloropyrimidine did not change the final product and only PNNP was obtained rather than the wanted complex, of which only one chlorine was substituted. However, if 1.5 equivalent *tert*-butyllithium based on Ph_2PH was used as base with the equivalent starting reactants, there were two products, disubstituted phosphine compound (PNNP) and asymmetrically substituted 4-*tert*-butyl-6-diphenylphosphino pyrimidine (PNN). The final products of the above reactions indicate that complex 4,6-dichloropyrimidine has high reactivity and low selectivity of the two chlorine

atoms. Ligand 2,6-bis(diphenylphosphino)pyridine (PNP) was prepared on the improved procedures according to the literature through the reaction of 2,6-dichloropyridine and lithium diphenylphosphide, which was produced by chlorodiphenyl phosphine and lithium in dry THF solution.[19] Besides, ligands PNNP and PNN are less stable than PNP, which brown slowly if they are exposed to the air.



Scheme 2 Synthetic routes for complexes 2-6.

As shown in Scheme 2, the mono-substituted tetranuclear derivatives **2** and **3**, were prepared via the reaction of $\text{Fe}_2(\mu\text{-pdt})(\text{CO})_6$ (**1**) with decarbonylation agent $\text{Me}_3\text{NO}\cdot 2\text{H}_2\text{O}$ followed by addition of $1/2$ equivalent PNP and PNNP in MeCN solution, respectively. In order to make a comparison, the corresponding mono-substituted dinuclear complexes **4** and **5** were synthesized, when one equivalent PNP and PNNP were used, respectively. Complex **6** was prepared in the

similar way as that for **4** or **5** but using one equivalent PNN as ligand. The crude products of **2-6** were all purified by chromatography on silica gel (100-200) in good to moderate yields.

Complexes synthesized were all characterized by ^1H NMR, ^{31}P NMR, infrared spectroscopy (IR), elemental analyses, ESI-MS spectrometry, and singlecrystal X-ray crystallography for **2**, **3** and **6**. Positive ion ESI-MS of the complexes showed the corresponding molecular ion peaks as the principal peaks.

The ^{31}P NMR spectra of **2**, **3** and **6** show one singlet at $\delta = 66.84$, 67.48 and 73.01 ppm, respectively. The value of **3** shifts to lower magnetic field by 0.64 ppm compared with that of **2**. This indicates that ligand PNNP is a slightly weaker electron donor than PNP. For the poorer electron-donating ability of PNN in **6** than that of PNNP in **3**, there is also a 5.53 ppm shift of **6** to lower magnetic field than that of **3**. In addition, the only one ^{31}P NMR signal observed in the spectrum of **2** or **3** suggests that the two P atoms in PNNP or PNP have the same chemical environment. There are two ^{31}P NMR peaks, 65.72 and -4.14 ppm for **4** and 66.51 and -3.76 ppm for **5**, respectively, corresponding to the ligated P atom and uncoordinated one in them.

The IR spectra of **2-6** each displays four characteristic peaks in the region of $1930\text{--}2049\text{ cm}^{-1}$, corresponding to the carbonyl stretching pattern for terminally bonded CO groups. The IR data of $\nu(\text{CO})$ of them, together with that of compound **1**, are listed in Table 2 for a clear comparison.

Table 2 Comparison of $\nu(\text{CO})$ bands in **2-6** with **1**.

Complexes	$\nu(\text{CO})\text{ KBr/cm}^{-1}$	$\nu_{1\text{st}}(\text{CO})^a\text{ KBr/cm}^{-1}$
1	2074, 2036, 1995	0
2	2041, 1977, 1985, 1933	33
3	2044, 1983, 1957, 1935	30
4	2042, 1979, 1956, 1930	32

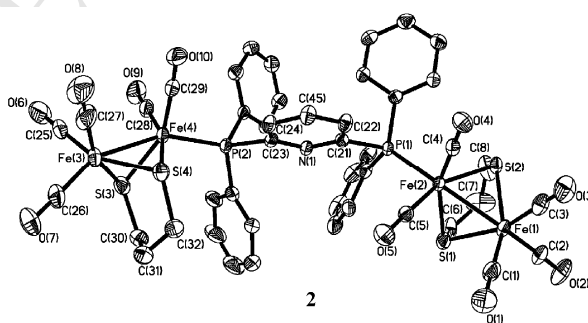
5	2044, 1982, 1955, 1931	30
6	2049, 1980, 1954, 1932	25

$$^a \nu_{1st}(\text{CO}) = \nu_{1st}(\text{CO})_1 - \nu_{1st}(\text{CO})_{\text{mono-substituted}}$$

For the electron-donating effects of phosphine ligands PNP, PNNP and PNN on the [FeFe] centers, CO bands in the IR spectra of **2-6** shift to lower energy compared to those of **1**. The addition of one N atom in ligand PNNP results in a 3 cm^{-1} blue-shift of the first (CO) band of **3** compared with that of **2**. The same trend can be observed for the dinuclear complex **5** compared with **4**. However, the comparable values of the first (CO) bands of PNP-substituted **2** and **4** (or PNNP-substituted **3** and **5**) indicate that the addition of another Fe_2S_2 unit to the ligand PNNP or PNP has little effect on the IR spectra.

3.2. Molecular Structures of **2**, **3** and **6**

The red crystals of **2**, and **3** suitable for X-ray diffraction were grown upon slow diffusion of hexane into dichloromethane solution at 4°C , and the one of **6** were grown upon diffusion of diethyl ether into a dichloromethane-methanol mixed solution containing **6** at 4°C . The crystallographic structures of **2**, **3** and **6** are displayed in Figure 1 and the selected bond lengths and angles are listed in Table S1 (Supporting Information). For the tetranuclear complexes **2**



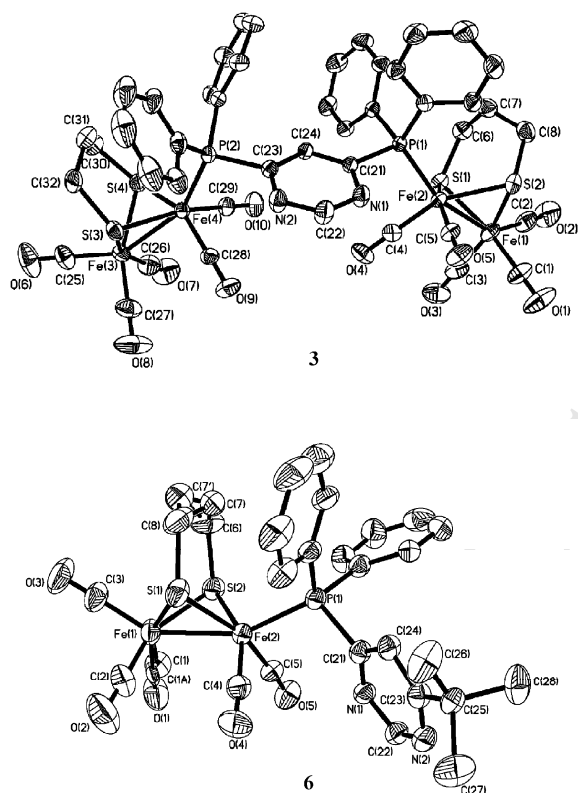


Figure 1 ORTEP views of complexes **2**, **3** and **6** with 30% probability level ellipsoids (the hydrogen atoms are omitted for clarity.).

and **3**, each Fe_2S_2 butterfly unit has a square pyramidal structure and is attached to one P atom of the diphosphine bridge. As the usual behaviour of the reported mono- or di-phosphine ligands,[33-36] each P atom of the diphosphine in **2** and **3** selected the apical position. However, the space group of **2** is $P-1$, which is different from $P21/n$ of **3**. Besides, both the tilts of the propanedithiolate rings in **2** are away from the ligand PNP, while the two six-membered rings of the propanedithiolate in **3** are towards PNNP moiety.

The Fe-Fe distances of **3** [2.5109(6) and 2.5188(6) Å] are comparable to that of $[(\mu\text{-pdt})\text{Fe}_2(\text{CO})_6]$ [2.5103(11) Å][37] and slightly shorter than those of **2** [2.5232(9) and 2.5209(10) Å]. But the Fe-Fe distance of each Fe_2S_2 unit in **2** is comparable, which suggests that the ligand

PNP has the same effect on the two linked Fe_2S_2 centers. The same trend can be concluded for PNNP in the complex **3**. For the dinuclear complex **6**, the structure is also the expected square-based-pyramidal coordination geometry and the P atom occupies an apical position as those in **2** and **3**. The middle C atom in $-\text{SCH}_2\text{CH}_2\text{CH}_2\text{S}-$ is disordered in two positions.

The crystal structures and metric data of $\text{Fe}\cdots\text{N}$ distances of **2**, **3** and **6** (Table S1) suggest that the N atoms in **2** and **3** are fixed and hardly swung due to the steric hindrance of two coordinated Fe_2S_2 units. But the orientations of the pyrimidyl-nitrogen atoms in **6** change to different positions compared to those in **3**. As shown in Table S1, the shortest $\text{Fe}\cdots\text{N}$ distance (3.585 Å) in the solid state is the one in complex **6**, which is also shorter than those using $\text{Ph}_2\text{PCH}_2\text{Py}$ and Ph_2PPy as mono-substituted ligands (3.919 and 3.653 Å, respectively).[38] Moreover, both of the distances of N atoms in pyrimidine ring to the nearest Fe atom in complex **3** (3.635, 3.859 Å) are apparently closer than those (4.492, 4.713 Å) in pyridine in **2**.

3.3. Electrochemical properties

3.3.1. Cyclic voltammograms of 2-6

Table 3 Reduction potentials of complexes **2-6** in CH_2Cl_2 or $\text{CH}_2\text{Cl}_2/\text{DMF}$ solutions.

Complexes	$E_{1/2}^{\text{red1}}$ (V) vs. Fc^+/Fc	$E_{1/2}^{\text{red2}}$ (V) vs. Fc^+/Fc
2	-2.06	---
3	-2.04	-2.25
4	-2.05	---
5	-2.02	-2.17
6 ^a	-1.83	-2.07

^a Mixed solution of $\text{CH}_2\text{Cl}_2/\text{DMF}$ (4:1) was used.

Cyclic voltammogram (CV) measurements were carried out on complexes **2-6** in dry CH_2Cl_2 or $\text{CH}_2\text{Cl}_2/\text{DMF}$ solutions for the poor solubility of **2**, **3** and **6** in Me_3CN . The reduction potentials of them are listed in Table 3 and all vs. Fc^+/Fc , unless otherwise noted.

PNP-substituted complexes **2** and **4** display irreversible reduction peaks at -2.06 and -2.05 V, respectively, in CH_2Cl_2 solutions. The comparable values suggest that the addition of another Fe_2S_2 unit to the ligand PNP has little effect on the reduction potential. Detailed experiments were carried out to study the reduction processes of them in THF solutions using 1mm diameter glassy carbon working electrode. The reduction wave of **2** splits into three peaks in THF solution (Figure S2a, Supporting Information). [16, 17] The first one is ascribed to the reduction of ligand PNP and the other couple of peaks are obviously the one-electron reduction processes of the two Fe_2S_2 centers as other PR_3 -monosubstituted diiron derivatives. [21, 39-42] This is somewhat different from the results of dppe-substituted tetranuclear complexes $[\{\mu\text{-(SCH}_2)_2\text{CH}_2\}\text{Fe}_2(\text{CO})_5(\text{Ph}_2\text{-PCH}_2)_2\}_2$ and $[\{\mu\text{-(SCH}_2)_2\text{N(CH}_2\text{CH}_2\text{CH}_3)\}\text{Fe}_2(\text{CO})_5(\text{Ph}_2\text{-PCH}_2)_2\}_2$, in which only the Fe_2S_2 centers are reduced by one step at ca. -2.0 V with consumptions of 2 electrons, respectively.

For the PNNP and PNN substituted complexes **3**, **5** and **6**, there are two reduction events for each one. The first reduction potentials of **3** and **5** are -2.04 V and -2.02 V, respectively, in CH_2Cl_2 solutions. The one of **6** in $\text{CH}_2\text{Cl}_2/\text{DMF}$ solution shifts positively to -1.83 V in $\text{CH}_2\text{Cl}_2/\text{DMF}$ solution. The second reduction potentials of **3**, **5** and **6** (-2.25, -2.17 and -2.07 V) are comparable to those of tetranuclear dppe-substituted complexes, which are ascribed to the reduction processes of $[\text{Fe}^\square\text{Fe}^\square]$ to $[\text{Fe}^\square\text{Fe}^0]$. Further CV experiments in THF show that the reduction waves of **3** splits to two couple of peaks, while there are only three ones of **5** for the absence of one $[\text{Fe}_2\text{S}_2]$ unit (Figure S2b, 2c, Supporting Information). Bulk electrolysis in

CH_2Cl_2 solutions indicates that complex **3** obtains 4.13 electrons, two for the reduction of ligand PNNP and the other two for the two $[\text{Fe}_2\text{S}_2]$ cores from $[\text{Fe}^\square\text{Fe}^\square]$ to $[\text{Fe}^\square\text{Fe}^0]$.^[43]

3.3.2. Electrocatalytic reduction of protons from acetic acid and trifluoroacetic acid with 2, 3 and 6 as catalysts.

Firstly, the protonation process of **3** was studied by ^{31}P NMR spectroscopy in CD_3Cl at room temperature. Figure 2 shows the variation of the ^{31}P resonances with the addition of 0-3 equiv. trifluoroacetic acid (TFA) to the solution of **3**.

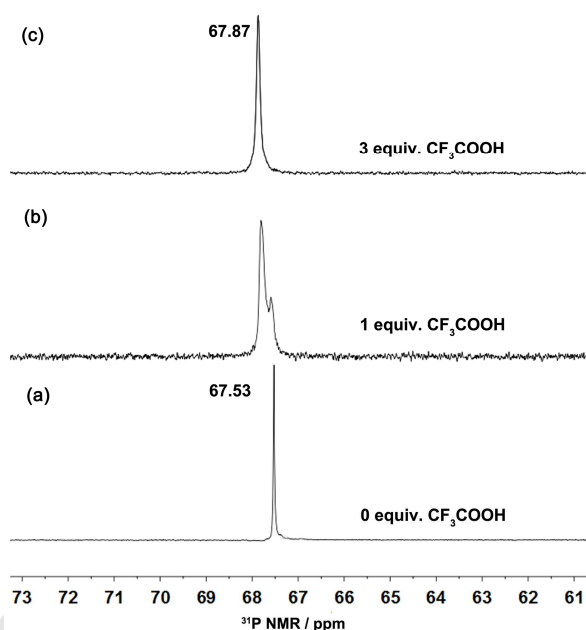
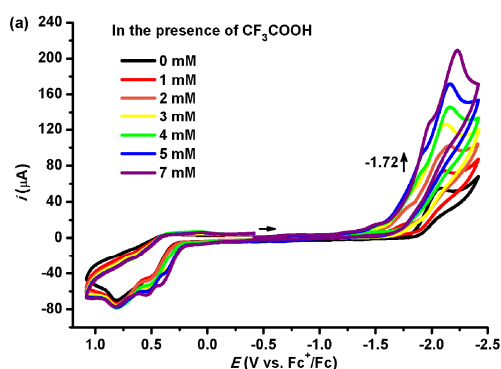


Figure 2 ^{31}P NMR spectra for the protonation of **3** in CD_3Cl at room temperature.

There is only one ^{31}P resonance at 67.53 ppm for PNNP in the complex **3** (Figure 2a). When 1 equiv. TFA is added, one additional sharp signal appears at 67.87 ppm (Figure 2b), which shifts only about 0.3 ppm to the low field compared with that of unprotonated PNNP in **3**. The only one additional signal suggests that both of the N atoms in PNNP are protonated and a new

species [**3**-2H_N] is generated. Upon addition of 3 equiv. TFA, the ³¹P signal of **3** completely disappears and only one ³¹P signal can be observed (Figure 2c). This implicates that complex **3** has been quantitatively transformed to the doubly protonated species [**3**-2H_N].

The cyclic voltammograms, mainly on complexes **2**, **3** and **6** in the presence of acetic acid (HOAc) and TFA, were carried out to investigate the electrocatalytic proton reduction processes. The current height of the reduction peak of **2** is slightly enhanced with an increase in the concentration of HOAc (Figure S3a, Supporting Information). The same trend can be observed for the first reduction event of **3**, whereas the second one remains almost unchanged (Figure S3b, Supporting Information). After HOAc is added to the solution of **6**, a new reduction peak is generated at about -1.71 V and the original two waves shift negatively to -1.96 and -2.12 V, respectively (Figure S3c). According to the reported pyridyl-phosphine monosubstituted derivatives,[38] the peak at -1.71 V can be ascribed to the reduction of the protonation of the pyrimidyl-nitrogen atom. The new wave keeps unchanged with the concentration of HOAc increasing, and the changes of the other two reduction processes are the same as those of complex **3**. It is worth noticing that there is no new reductive event for the tetranuclear complex **3**, which also contains pyrimidyl ligand.



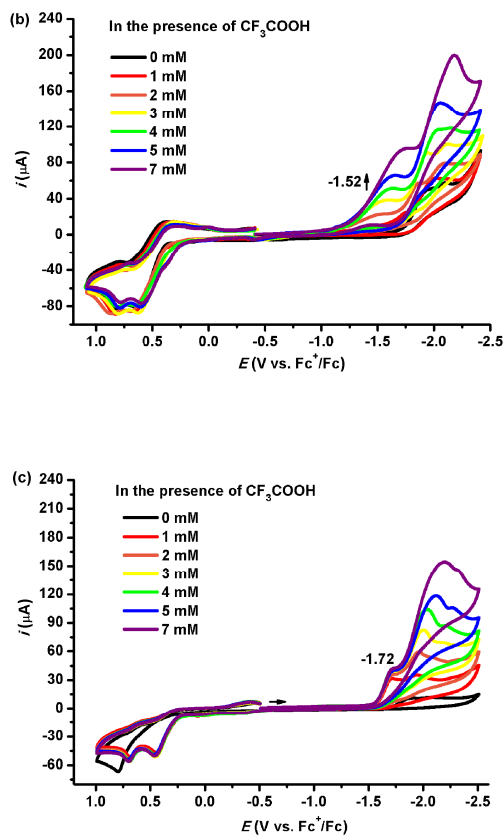


Figure 3 Cyclic voltammograms of **2** (a), **3** (b) and **6** (c) (1.0 mM) in the presence of CF_3COOH at scan rate of 100 mV s^{-1} in $0.1\text{M n-Bu}_4\text{NPF}_6 \text{ CH}_2\text{Cl}_2$ solutions.

When TFA is used, the current heights of the reduction events of **2**, **3** and **6** are enhanced greatly (Figure 3). Moreover, new reductive waves are observed at -1.72 V for **2**, -1.52 V for **3** and -1.72 V for **6**, respectively, which result from the protonation of the pyridyl-nitrogen atom and pyrimidyl-nitrogen atoms. Complexes **2** and **3** display similar CV features upon the addition of TFA in the range of 0-7 mM. The current heights increase with the addition of TFA with potentials negatively shifting. As shown in Figure 3, there are 200 mV positive shifts for the first reduction process of $[\mathbf{3}\text{-}2\text{H}_\text{N}]$ compared with those of $[\mathbf{2}\text{-H}_\text{N}]$ and $[\mathbf{6}\text{-}2\text{H}_\text{N}]$, which indicates that $[\mathbf{3}\text{-}2\text{H}_\text{N}]$ is much easier to be reduced. We consider the ligand PNNP in complex **3** as a special

“bridge”, which can influence the electron character of the whole complex, when the two P atoms are both coordinated to metal centers.

3.4. DFT computational studies

The density functional theory (DFT) method was employed in the Gaussian 03 program to get an in-depth understanding of the electron characters of complexes **2-6**. The energies of the selected molecular orbitals (MOs) and the component (%) to the MO in terms of the composing units are listed in Table S2. The plots of the highest occupied molecular orbitals (HOMOs) and lowest unoccupied molecular orbitals (LUMOs) of **2**, **3** and **6** are displayed in Figure 5 and those of **4**, **5** and the protonated species [**2-H_N**], [**3-2H_N**] and [**6-2H_N**] are shown in Figure S4 for a comparison. As shown in Table S2, the LUMO orbital energy of **3** is -0.20 eV lower than that of **2**, suggesting that it is easier for **3** to accept an electron than **2**.

The major contributions to the HOMOs of **2-6** are all from one diiron unit together with the surrounding P atoms (Table S2). The LUMO of **2** is mainly resident on one Fe₂S₂ center (78.1%) along with the ligated PPh₂ unit (9.57%), while the other Fe₂S₂ and the pyridyl contribute only a little. Similar results of the PNP-substituted dinuclear complex **4** can be obtained. However, the contributions

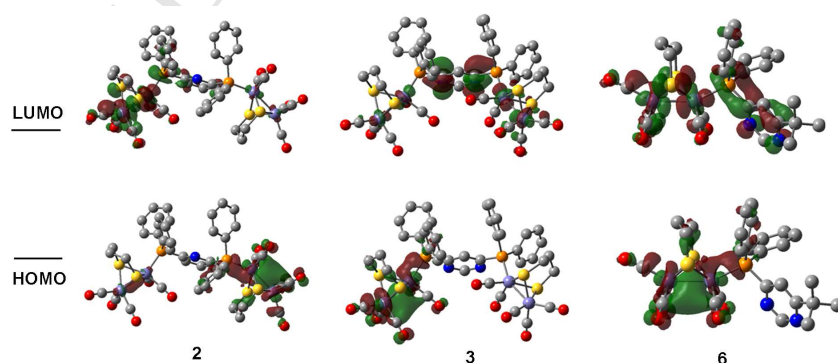


Figure 5 Plots of the HOMO and LUMO orbitals of complexes **2**, **3** and **6** in the ground state by DFT method at the B3LYP level (isovalue = 0.03) (the hydrogen atoms are omitted for clarity).

to the LUMO of **3** are comparable from the two Fe_2S_2 centers (30.75% and 31.43%) and ligated PNNP (37.82%), which also can be seen from the plot shown in Figure 5. This suggests that electron injected may delocalize in the whole complex of **3**. Moreover, when only one P atom in PNNP is coordinated (**5**), the primary contribution to LUMO is from the diiron core (77.49%), while the contribution from ligand PNNP lowers down to 22.51%. Complex **6** has similar result, and the contributions from Fe_2S_2 core and ligand PNN are 77.34% and 22.66%, respectively. The differences between the contributions to LUMOs of PNNP-substituted tetranuclear **3** and dinuclear **5** indicate that the model of metal-PNNP-metal (M-PNNP-M) can make the contribution to LUMO come from the whole molecular **3**. The differences between the LUMOs of pyrimidyl and pyridyl phosphine-substituted complexes may explain why two reduction processes were observed in **3**, **5** and **6** and only one for **2** and **4**.

The LUMO orbital energies of protonated [**2-H_N**], [**3-2H_N**] and [**6-2H_N**] are -3.45, -5.08 and -4.59 eV, respectively, as shown in Table S2. The lower LUMO orbital energy of [**3-2H_N**] suggests an easier acceptance of electrons for it. Figure S4 shows the contributions to LUMOs of them are all mainly from the protonated pyrimidyl or pyridyl groups. Those results further evidence the adsorption of the first reduction events of complexes **2**, **3** and **6** in Figure 3.

4 Conclusions

In this work, a pyrimidyl group is firstly introduced to the phosphine ligand and two new ligands, PNNP and PNN, have been designed and synthesized depending on the reaction conditions. These two ligands together with the pyridyl ligand PNP were reacted with $\text{Fe}_2(\mu-$

pd)(CO)₆ to give the mono-substituted derivatives **2-6**. The crystal structures of tetranuclear iron-sulfur complexes **2** and **3** occupy different space groups (*P-1* and *P21/n*, respectively) due to the different bridges between the two Fe₂S₂ units in them. For the stronger electron-withdrawing inductive and conjugative effect of the two N atoms in pyrimidyl ring than that in pyridyl, the electron characters of PNNP- or PNN-substituted derivatives are different from that of PNP-substituted ones. Complexes **3**, **5** and **6** containing pyrimidyl display two reduction waves; one is ascribed to the reductive process of diiron center, the other is the reduction of the pyrimidyl unit. While both of the PNP-substituted complexes **2** and **4** show only one reductive wave of Fe^IFe⁰/Fe^IFe^I. The theoretical studies of PNP-substituted **2** and **4**, PNNP-substituted dinuclear **5** and PNN-substituted **6** demonstrate that the contributions to LUMOs mainly come from one Fe₂S₂ unit along with the surrounded P atoms. But for the PNNP-substituted tetranuclear complex **3**, the LUMO is comparably resident on the whole molecular.

Acknowledgements

This investigation was based on work supported by the National Natural Science Foundation of China (Nos. 21101153, 21231003, 21203195 and 21303201).

Appendix A. Supplementary data

The supplementary crystallographic data have been deposited at the Cambridge Crystallographic Data Center as .cif files, with CCDC number 970444, 970445 and 970446. These data can be obtained free of charge via www.ccdc.cam.ac.uk/data_request/cif. Supporting Figures and CIF files giving the electrochemistry, DFT computational studies can be found in the online version.

References

- [1] C. Tard, C.J. Pickett *Chem. Rev.* 109 (2009) 2245–2274.
- [2] G.A.N. Felton, C.A. Mebi, B.J. Petro, A.K. Vannucci, D.H. Evans, R.S. Glass, D.L. Lichtenberger *J. Organomet. Chem.* 694 (2009) 2681–2699.
- [3] J.I. Van Der Vlugt, T.B. Rauchfuss, S.R. Wilson *Chem. Eur. J.* 12 (2005) 90–98.
- [4] D. Chong, I.P. Georgakaki, R. Mejia-Rodriguez, J. Sanabria-Chinchilla, M.P. Soriaga, M.Y. Darensbourg *Dalton Trans.* 21 (2003) 4158–4163.
- [5] L. Schwartz, G. Eilers, L. Eriksson, A. Gogoll, R. Lomoth, S. Ott *Chem. Commun.* 5 (2006) 520–522.
- [6] G. Si, W.G. Wang, H.Y. Wang, C.H. Tung, L.Z. Wu *Inorg. Chem.* 47 (2008) 8101–8111.
- [7] W.F. Liaw, N.H. Lee, C.H. Chen, C.M. Lee, G.H. Lee, S.M. Peng *J. Am. Chem. Soc.* 122 (2000) 488–494.
- [8] S. Ezzaher, J.F. Capon, F. Gloaguen, F.Y. Pétilion, P. Schollhammer, J. Talarmin, N. Kervarec *Inorg. Chem.* 48 (2009) 2–4.
- [9] S. Ghosh, G. Hogarth, N. Hollingsworth, K.B. Holt, I. Richards, M.G. Richmond, B.E. Sanchez, D. Unwin *Dalton Trans.* 42 (2013) 6775–6792.
- [10] W.G. Wang, M.J. Nilges, T.B. Rauchfuss, M. Stein *J. Am. Chem. Soc.* 135 (2013) 3633–3639.
- [11] D. Chouffai, G. Zampella, J.F. Capon, L. De Gioia, F. Gloaguen, F.Y. Pétilion, P. Schollhammer, J. Talarmin *Inorg Chem* 50 (2011) 12575–12585.
- [12] L.C. Song, Z.Y. Yang, H.Z. Bian, Q.M. Hu, *Organometallics* 23 (2004) 3082–3084.
- [13] Y.T. Si, K. Charreter, J.F. Capon, F. Gloaguen, F.Y. Pétilion, P. Schollhammer, J. Talarmin *J. Inorg Biochem* 104 (2010) 1038–1042.

- [14] J. F. Capon, F. Gloaguen, P. Schollhammer, J. Talarmin *J. Electroanal. Chem.* 595 (2006) 47–52.
- [15] G.A.N. Felton, A.K. Vannucci, J.Z. Chen, L.T. Lockett, N. Okumura, B.J. Petro, U.I. Zakai, D.H. Evans, R.S. Glass, D.L. Lichtenberger *J. Am. Chem. Soc.* 129 (2007) 12521–12530.
- [16] L. Chen, M. Wang, F. Gloaguen, D.H. Zheng, P.L. Zhang, L.C. Sun *Inorg. Chem.* 52 (2013) 1798–1806.
- [17] L. Chen, M. Wang, F. Gloaguen, D.H. Zheng, P.L. Zhang, L.C. Sun *Chem. Eur. J.* 18 (2012) 13968–13973.
- [18] G.R. Newkome, D.W. Evans, F.R. Fronczek *Inorg. Chem.* 26 (1987) 3500.
- [19] F.E. Wood, M.M. Olmstead, A.L. Balch *J. Am. Chem. Soc.* 105 (1983) 6334–6335.
- [20] R. Hourihane, G. Gray, T. Spalding, T. Deeney *J. Organomet. Chem.* 642 (2002) 40–47.
- [21] P. Li, M. Wang, C.J. He, G.G. Li, X.Y. Liu, C.N. Chen, B. Åkermark, L.C. Sun *Eur. J. Inorg. Chem.* 2005 2506–2513.
- [22] Q.Y. Xing, W.W. Pei, R.Q. Xu, J. Pei *Basic Organic Chemistry*, third ed., Higher Education Press, Beijing, **2005**.
- [23] A. Winter, L. Zsolnai, G.Z. Huttner, *Naturforsch.* 37b (1982) 1430–1436.
- [24] G.M. Sheldrick SADABS, University of Göttingen: Göttingen, Germany, (1996).
- [25] G.M. Sheldrick SHELXTL. Version 5.1, Siemens Analytical X-ray Instruments Inc., Madison, Wisconsin, USA, (1994).
- [26] M. J. Frisch, G. W. Trucks, H. B. Schlegel, G. E. Scuseria, M. A. Robb, J. R. Cheeseman, J. A. Montgomery, T. Vreven, K. N. Kudin, J. C. Burant, J. M. Millam, S. S. Iyengar, J. Tomasi, V. Barone, B. Mennucci, M. Cossi, G. Scalmani, N. Rega, G. A. Petersson, H. Nakatsuji, M. Hada, M. Ehara, K. Toyota, R.; Fukuda, J. Hasegawa, M. Ishida, T. Nakajima,

- Y. Honda, O.; Kitao, H. Nakai, M. Klene, X. Li, J. E. Knox, H. P. Hratchian, J. B. Cross, C. Adamo, J. Jaramillo, R. Gomperts, R. E. Stratmann, O. Yazyev, A. J. Austin, R. Cammi, C. Pomelli, J. W. Ochterski, K. Morokuma, G. A. Voth, P. Salvador, J. J. Dannenberg, V. G. Zakrzewski, S. Dapprich, A. D. Daniels, M. C. Strain, O. Farkas, D. K. Malick, A. D. Rabuck, K. Raghavachari, J. B. Foresman, J. V. Ortiz, Q. Cui, A. G. Baboul, S. Clifford, J. Cioslowski, B. B. Stefanov, G. Liu, A. Liashenko, P. Piskorz, I. Komaromi, R. L. Martin, D. J. Fox, T. Keith, M. A. Al-Laham, C. Y. Peng, A. Nanayakkara, M. Challacombe, P. M. W. Gill, B. Johnson, W.; Wong, M. W. Chen, C. Gonzalez and J. A. Pople, Gaussian 03, revision D.02. Gaussian, Inc.: Wallingford, CT, 2004.
- [27] A.D. Becke *J. Chem. Phys.* 98 (1993) 5648-5652.
- [28] C.T. Lee, W.T. Yang, R.G. Parr *Phys. Rev. B* 37 (1988) 785–789.
- [29] V. Barone, M. Cossi *J. Phys. Chem. A* 102 (1998) 1995–2001.
- [30] M. Cossi, N. Rega, G. Scalmani, V. Barone, *J. Comput. Chem.* 24 (2003) 669–681.
- [31] P. Ros, G.C.A. Schuit *Theo. Chim. Acta (Berl.)* 4 (1966) 1–12.
- [32] T. Lu, F.W. Chen *J. Comp. Chem.* 33 (2012) 580–592.
- [33] X. Zhao, I.P. Georgakaki, M.L. Miller, R. Mejia-Rodriguez, C.Y. Chiang, M.Y. Darensbourg *Inorg. Chem.* 41 (2002) 3917-3928.
- [34] W. Gao, J. Liu, B. Åkermark, L.C. Sun *Inorg. Chem.* 45 (2006) 9169-9171.
- [35] F. Gloaguen, J.D. Lawrence, T.B. Rauchfuss, M. Benard, M.M. Rohmer *Inorg. Chem.* 41 (2002) 6573–6582.
- [36] S. Ott, M. Borgström, M. Kritikos, R. Lomoth, J. Bergquist, B. Åkermark, L. Hammarström, L.C. Sun *Inorg. Chem.* 43 (2004) 4683–4692.

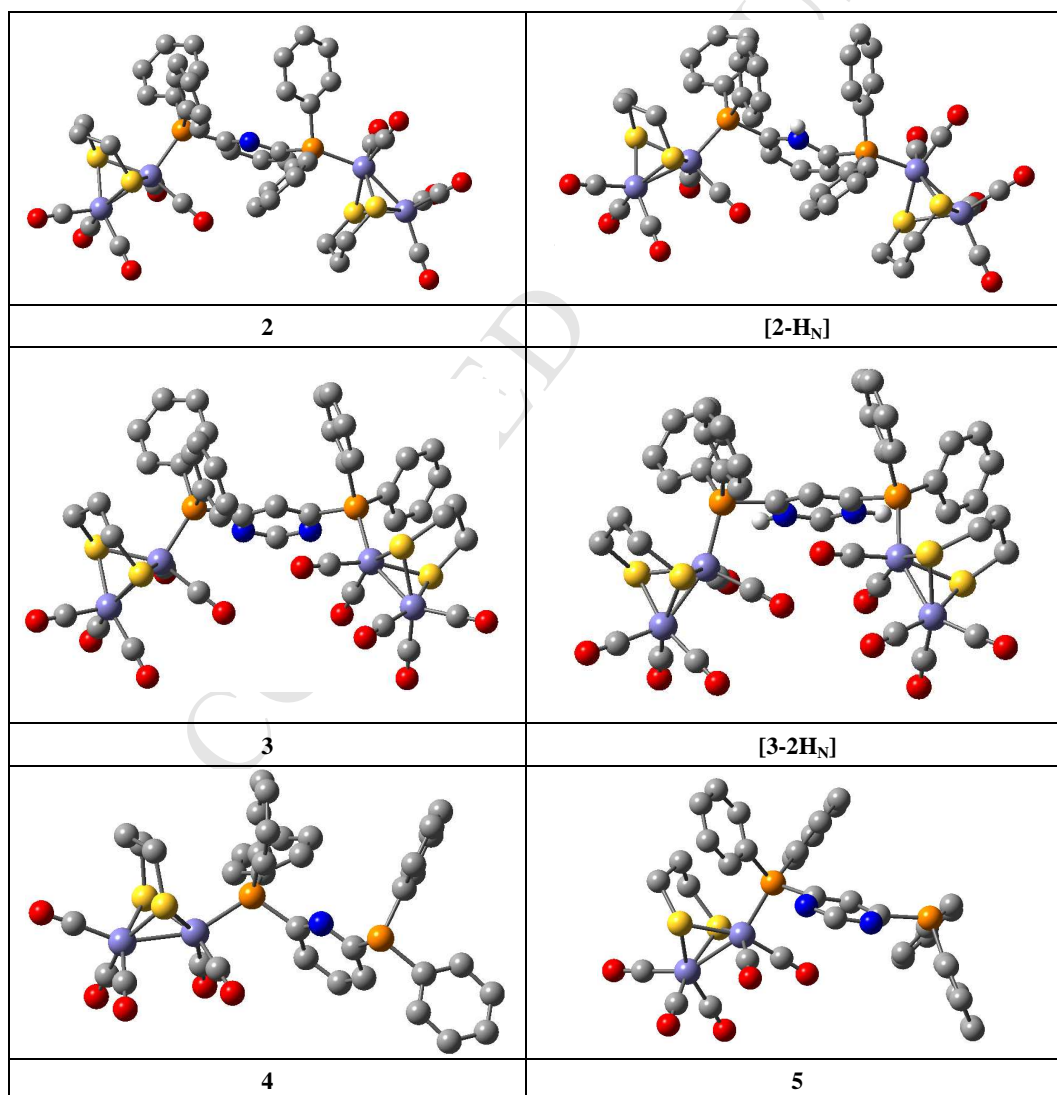
- [37] F. Gloaguen, J.D. Lawrence, M. Schmidt, S.R. Wilson, T.B. Rauchfuss *J. Am. Chem. Soc.* 123 (2001) 12518–12527.
- [38] P. Li, M. Wang, L. Chen, J.H. Liu, Z.B. Zhao, L.C. Sun *Dalton Trans.* 11 (2009) 1919–1926.
- [39] J.F. Capon, S.E. Hassnaoui, F. Gloaguen, P. Schollhammer, J. Talarmin *Organometallics* 24 (2005) 2020–2022.
- [40] T. Li, M.Y. Darensbourg *J. Am. Chem. Soc.* 129 (2007) 7008–7009.
- [41] D. Morvan, J.F. Capon, F. Gloaguen, A. Le Goff, M. Marchivie, F. Michaud, P. Schollhammer, J. Talarmin, J.J. Yaouanc, R. Pichon, N. Kervarec *Organometallics* 26 (2007) 2042–2052.
- [42] S. Ezzaher, P.Y. Orain, J.F. Capon, F. Gloaguen, F.Y. Pétilion, T. Roisnel, P. Schollhammer, J. Talarmin *Chem. Commun.* 27 (2008) 2547–2549.
- [43] W.M. Gao, J.E. Bjo1m, J.H. Liu, C.N. Chen, L. Eriksson, L.H. Weng, L. Åkermark, L.C. Sun *Inorg. Chem.* 46 (2007) 1981–1991.

Supporting Information

Pyridyl- and Pyrimidyl-Phosphine-Substituted [FeFe]-Hydrogenase Mimics: Synthesis, Characterization and Properties

Hong-Hua Cui,^{a,b} Nan-Nan Wu,^{a,b} Jin-Yun Wang,^a Ming-Qiang Hu,^a Hui-Min Wen,^a Xiao-Wei Song,^{a,b}
and Chang-Neng Chen*^a

^aState Key Laboratory of Structural Chemistry, Fujian Institute of Research on the Structure of Matter, Chinese Academy of Sciences, Fuzhou 350002, P. R. China. ^bUniversity of Chinese Academy of Sciences, Beijing, 100039, P. R. China. E-mail: ccn@fjirsm.ac.cn.



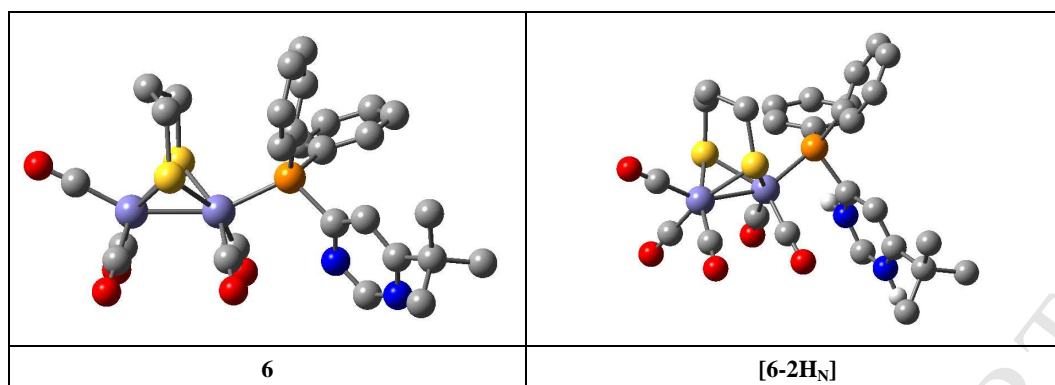


Figure. S1. The optimized structures of complexes **2-6** and protonated [**2-H_N**], [**3-2H_N**] and [**6-2H_N**] in the ground state by DFT method at the B3LYP level. Purple, yellow, orange, red, blue, and gray spheres represent the iron, sulfur, phosphorus, oxygen, nitrogen, and carbon atoms, respectively. For clarity, the hydrogen atoms are omitted.

Table S1 Selected bond lengths (Å) and angles (degrees) for complexes **2**, **3** and **6**.

Complexes	2	3	6
Fe(1)–C(1)	1.766(6)	1.794(4)	1.78(3)
Fe(1)–C(2)	1.813(5)	1.789(4)	1.752(9)
Fe(1)–C(3)	1.802(6)	1.795(5)	1.792(7)
Fe(2)–C(4)	1.772(5)	1.771(3)	1.784(6)
Fe(2)–C(5)	1.773(4)	1.775(3)	1.780(6)
Fe(2)–S(1)	2.2626(14)	2.2606(8)	2.273(3)
Fe(2)–S(2)	2.2623(12)	2.2714(9)	2.276(2)
Fe(4)–S(3)	2.2692(14)	2.2575(8)	-----
Fe(4)–S(4)	2.2656(14)	2.2721(9)	-----
Fe(2)–P(1)	2.2315(11)	2.2155(7)	2.254(2)
Fe(4)–P(2)	2.2290(12)	2.2184(8)	-----
Fe(2)–Fe(1)	2.5232(9)	2.5109(6)	2.542(3)
Fe(4)–Fe(3)	2.5209(10)	2.5188(6)	-----
Fe---N ^a	4.713	3.635	3.585
	4.492	3.859	5.72
Fe(2)–S(1)–Fe(1)	67.78(4)	67.51(2)	67.77(8)
Fe(1)–S(2)–Fe(2)	67.77(4)	67.40(3)	67.83(8)

^a The Fe atoms are the ones only in one [Fe₂S₂] unit.

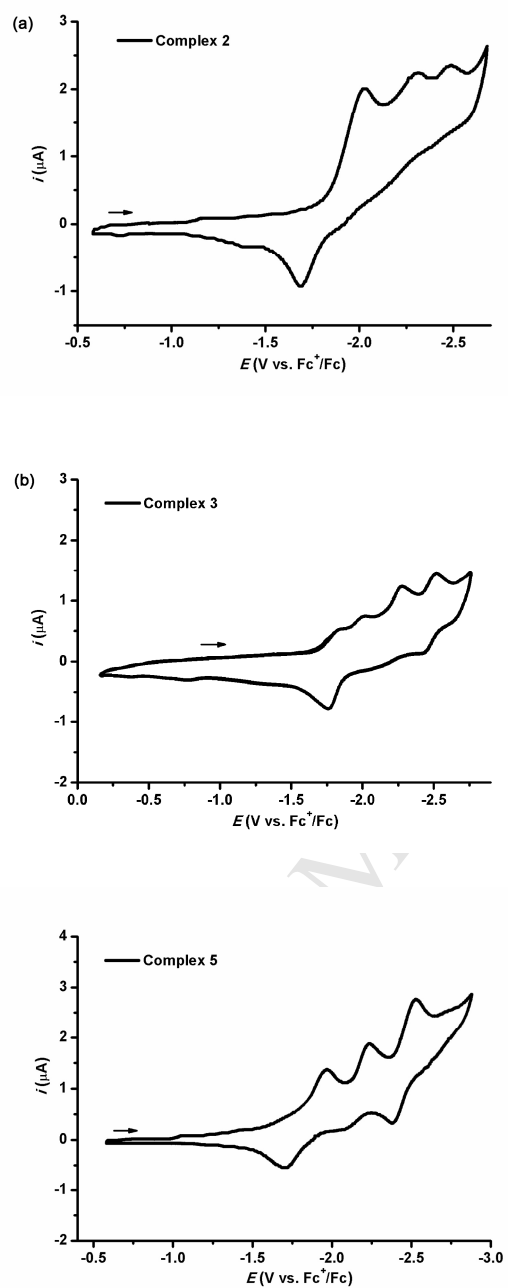


Figure. S2 Cyclic voltammograms of **2** (a), **3** (b) and **5** (c) (0.25mM) in 0.1M $n\text{-Bu}_4\text{NPF}_6$ in THF solutions at a scan rate of 100 mV s^{-1} .

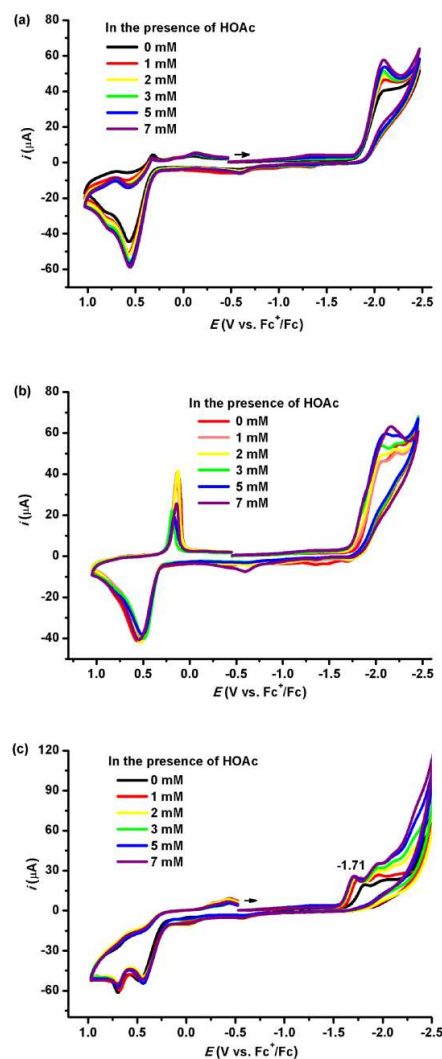
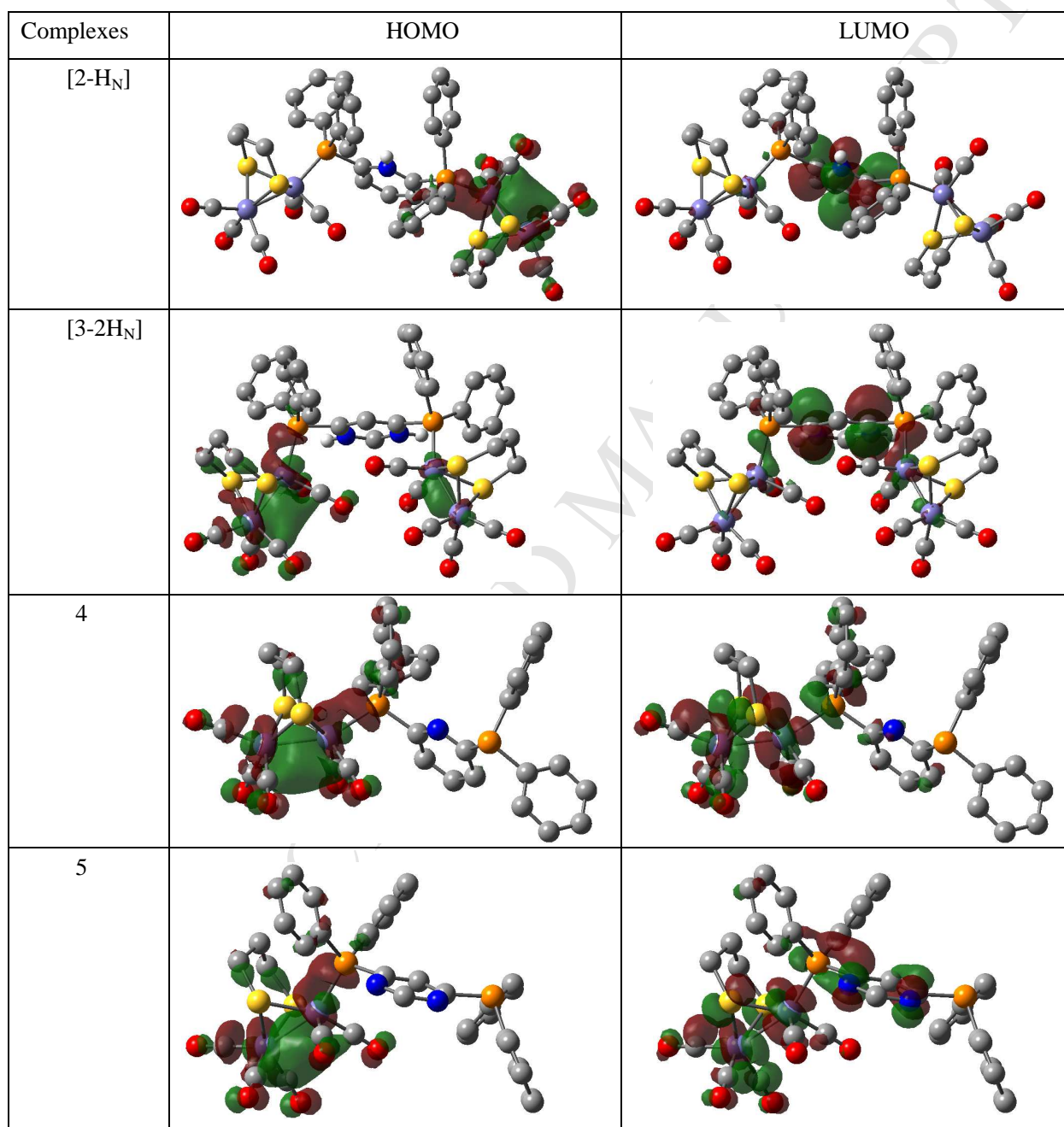


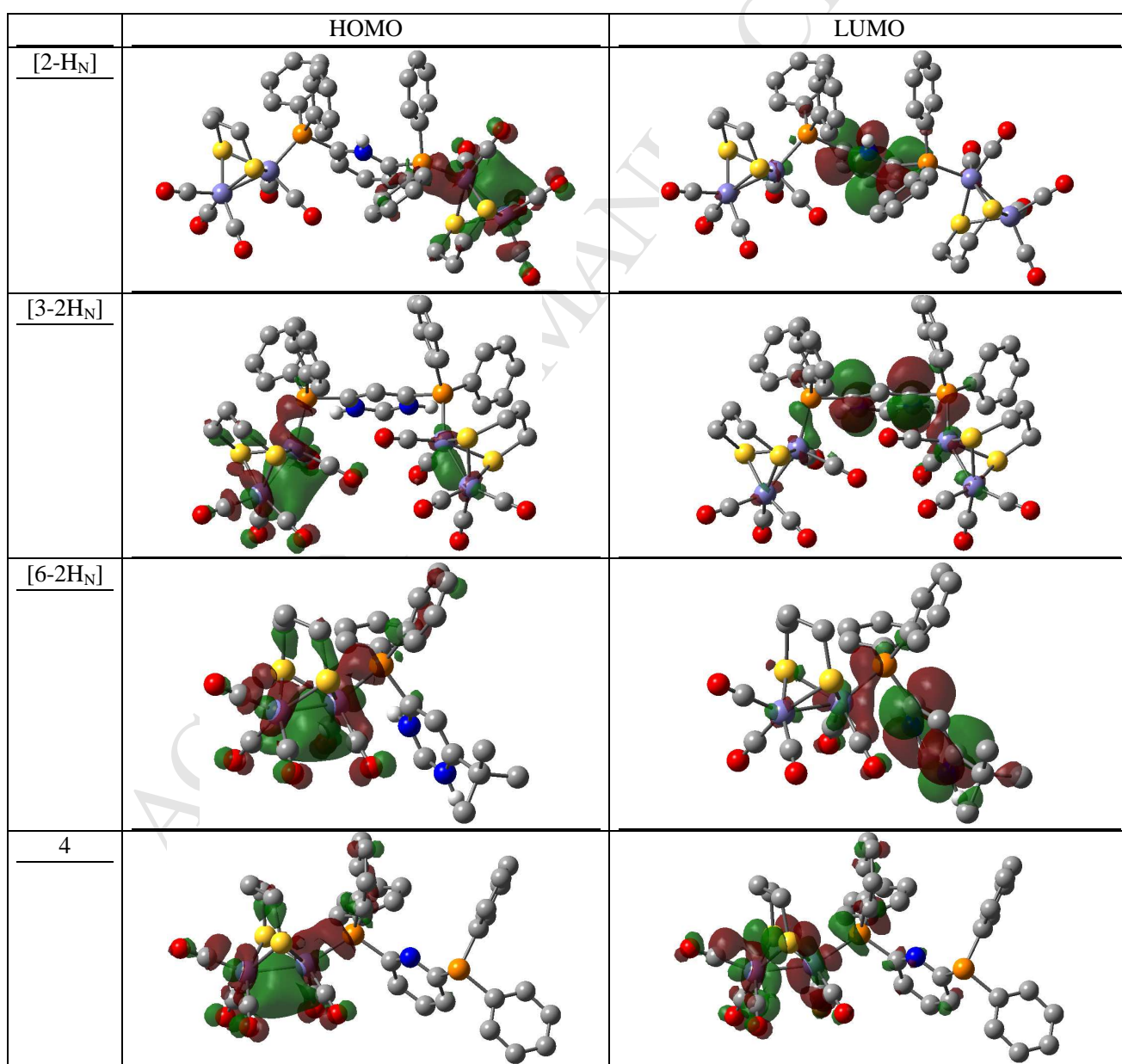
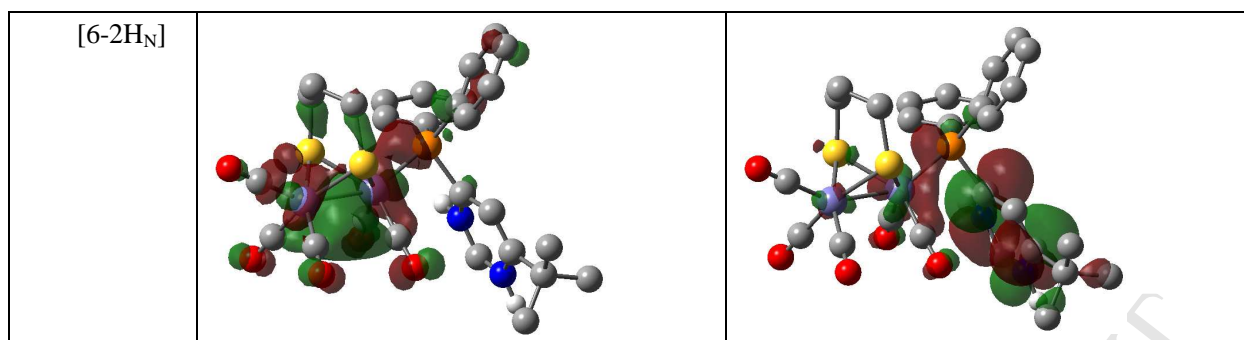
Figure. S3 Cyclic voltammograms of **2** (a), **3** (b) and **6** (c) in the presence of HOAc at a scan rate of 100 mV s^{-1} in CH_2Cl_2 or $\text{DMF}/\text{CH}_2\text{Cl}_2$ (**6**) solutions.

Table S2 The partial molecular orbital compositions (%) of complexes **2–6** and and protonated [**2-H_N**], [**3-2H_N**] and [**6-2H_N**] by SCPA approach (C-squared population analysis proposed by Ros and Schuit) calculated by DFT method at the B3LYP level.

Complexes	Orbitals	Energy (eV)	Molecular Component (%)				
			Fe_2S_2 -left	PPh_2 -left	Py./Pyr.	PPh_2 -right	Fe_2S_2 -right
2	LUMO	-1.96	78.10	9.57	4.54	1.22	6.57
	HOMO	-5.77	7.13	1.18	1.10	10.89	79.70
[2-H_N]	L	-3.45	4.14	3.06	73.87	8.64	10.29
	H	-6.25	0.21	0.07	0.92	12.53	86.26
3	L	-2.16	30.75	7.33	25.55	4.94	31.43
	H	-5.75	88.14	10.31	0.80	0.13	0.62
[3-2H_N]	L	-5.08	6.70	7.04	69.25	7.50	9.51
	H	-6.77	74.00	8.24	0.97	2.38	14.41
4	L	-1.88	86.74	9.93	3.23	0.10	----
	H	-5.73	85.78	12.20	1.42	0.60	----

5	L	-2.01	77.49	8.74	11.83	1.95	----
	H	-5.76	88.12	10.77	0.69	0.43	----
6	L	-1.95	77.34	11.37	10.26	1.03	----
	H	-5.77	88.99	10.29	0.68	0.04	----
[6-2H _N]	L	-4.59	21.84	9.74	63.17	5.25	
	H	-7.29	86.06	11.74	2.04	0.16	





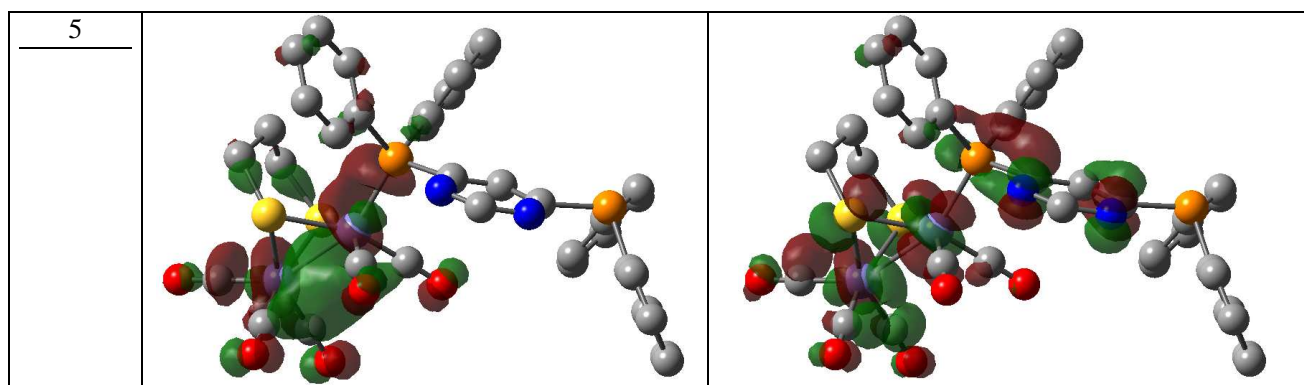


Figure. S4 The plots of the HOMOs and LUMOs of complexes 4, 5 and the protonated [2-H_N], [3-2H_N] and [6-2H_N].